Hybrid Resolution Spectral Imaging by Class-based Regression Method

Yuri Murakami[1], Masahiro Yamaguchi[2], and Nagaaki Ohyama[1]; [1]Imaging Science & Engineering Laboratory, Tokyo Institute of Technology; Yokohama, Japan, [2]Global Scientific Information and Computing Center, Tokyo Institute of Technology; Tokyo, Japan

Abstract

Hybrid resolution spectral imaging produces spectral images from high-resolution RGB images and corresponding low-resolution spectral data. Various methods have been proposed, whereas the low-resolution spectral data are regarded as the sample data of target scenes. However, this approach is not appropriate when each spectrum in the low-resolution data may be a mixture of spectra with different spectral features, and the original spectral feature is lost by averaging them. To solve this problem, class-based regression method for mixed low-resolution spectral data was proposed. In this method, the spectral estimation matrix for every class is derived using a regression approach, where the clustering results of the high-resolution RGB image are used to incorporate spectral unmixing. However, the method was tested only for small regions of images. In this paper, spectral images are estimated by the class-based regression method for three test spectral images, and the accuracy is compared with two conventional methods for hybrid resolution spectral imaging. Experiments confirm that the spectra are accurately reconstructed only by class-based regression method when they are observed as mixed spectra in the low-resolution data.

Introduction

The concept of hybrid resolution spectral imaging was originally proposed by Imai and Berns [1], and it has progressed as a new type of spectral imaging schemes recently [2-5]. In these schemes, spectral images are estimated from two types of data with different spatial and spectral resolutions: high-resolution RGB images and corresponding low-resolution spectral data, for instance (Fig.1). Various estimation methods were proposed mainly for the above-mentioned combination of data.

In the field of remote sensing, similar recovery techniques from multisensor data sets have already been studied, and they are called "image fusion (merging)" [6-8]. However, in the field of color imaging, this image fusion technique is only recently introduced.

The methods, previously proposed by the authors [2-4], define one or more linear mapping matrices from the RGB data to the spectra, which are generated by using low-resolution spectral data as training data. Then, a spectral image is estimated from its corresponding high-resolution RGB image by the derived mapping matrices. However, in some cases, it is not appropriate for the measured low-resolution spectral data to be used as training data of the scene spectra as described below.

Low-resolution spectral data are supposed to be measured by averaging over some area. This area often will be larger than the pixel size of the high-resolution RGB images because measurement of spectra over a larger area increases light energy sampled. If various spectra with different spectral shapes are located in a relatively small region, these different spectra are
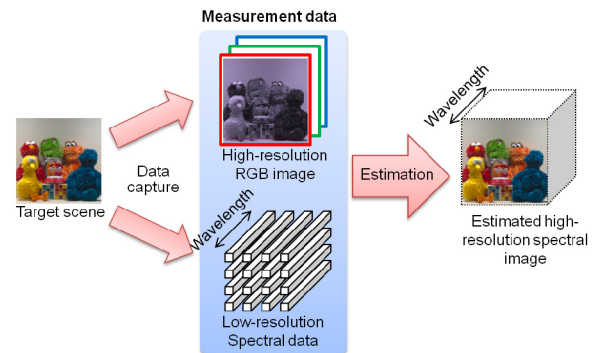
Figure 1. *Conceptual diagrams of hybrid resolution spectral imaging for high-resolution RGB images and low-resolution spectral data.*

averaged and measured as a single set of data at low resolution. As a result, some spectral features of original spectral scenes can be lost.

Estimating pure spectra from a mixed spectrum is a classic problem called "spectral unmixing" in the field of remote sensing [9]. In addition, the combination of spectral unmixing and image fusion techniques has been investigated as unmixing-based fusion [10,11]. However, the mixing models used in these methods are not necessarily appropriate to represent gradational color changes, which often appear in natural scene images.

To solve this problem, recently, a class-based regression method was proposed for hybrid resolution spectral imaging [12]. This method designs spectral estimation matrices considering that low-resolution spectral data are assumed to be mixtures of the spectra from multiple classes. The preliminary experiments showed that the spectral were accurately reconstructed even when they were observed as mixed spectra in the low-resolution data. However, the method was tested only for small regions of images.

In this paper, class-based regression method is applied to three test images, and the accuracy is compared with two conventional methods for hybrid resolution spectral imaging.

Hybrid resolution spectral imaging by class-based regression method
Numerical model for hybrid resolution spectral imaging

Let us introduce the image formation, which is assumed in the hybrid resolution spectral imaging discussed in this paper. It is assumed that a data acquisition system produces a high-resolution *B*-band image (*B*=3 in the case of RGB images) without spatial degradation and a low-resolution spectral image without spectral degradation from the same original image of spectral reflectance.

In addition, these two images are supposed to be spatially registered. For simplicity, the original spectral image is treated as discrete signals below.

Let $\mathbf{f}(i)$ be an L-dimensional column vector representing the spectral reflectance function of the original spectral reflectance image at pixel i, where L is the number of spectral samplings, and $1 \le i \le N = N_1 \times N_2$. The original spectral reflectance image is represented by an $L \times N$ matrix,

$$\mathbf{F} = [\mathbf{f}(1), \mathbf{f}(2), \cdots, \mathbf{f}(i), \cdots, \mathbf{f}(N)] \tag{1}$$

Digital imaging devices can be modeled as linear systems if the nonlinearity of the system is adequately corrected. Then, the B-band image signal $\mathbf{g}(i)$ corresponding to $\mathbf{f}(i)$ is represented by

$$\mathbf{g}(i) = \mathbf{H}_G \mathbf{f}(i) + \boldsymbol{\varepsilon}_G(i) \tag{2}$$

where $\mathbf{H}_G$ is a $B \times L$ system matrix comprising the spectral characteristics of the camera and the illumination spectrum, and $\boldsymbol{\varepsilon}_G(i)$ is a B-dimensional noise vector. In Eq. (2), it is assumed that there is no spatial degradation. The whole B-band image $\mathbf{G} = [\mathbf{g}(1), \mathbf{g}(2), \cdots, \mathbf{g}(N)]$ is given by

$$\mathbf{G} = \mathbf{H}_G \mathbf{F} + \mathbf{E}_G \tag{3}$$

where $\mathbf{E}_G = [\boldsymbol{\varepsilon}_G(1), \boldsymbol{\varepsilon}_G(2), \cdots, \boldsymbol{\varepsilon}_G(N)]$.

Let $\mathbf{s}(j)$ be an L-dimensional column vector representing the spectral data of a low-resolution spectral image at pixel j ($1 \le j \le M = M_1 \times M_2$). Let Ω_j be the area in the original spectral image corresponding to the j-th pixel of the low-resolution spectral image. Then, assuming that the spectral reflectance functions included in Ω_j are spatially averaged and observed without spectral degradation,

$$\mathbf{s}(j) = \sum_{i \in \Omega_j} \mathbf{f}(i) + \boldsymbol{\varepsilon}_S(j) \tag{4}$$

where $\boldsymbol{\varepsilon}_S(j)$ is an L-dimensional noise vector, and the spatial sensitivity of the spectral sensor is assumed to be uniform. If we define an $N \times M$ matrix $\mathbf{H}_S$ as

$$[\mathbf{H}_S]_{ij} = \begin{cases} 1 & i \in \Omega_j \\ 0 & else \end{cases}, \tag{5}$$

then the whole low-resolution spectral image $\mathbf{S} = [\mathbf{s}(1), \mathbf{s}(2), \cdots, \mathbf{s}(M)]$ is

$$\mathbf{S} = \mathbf{F} \mathbf{H}_S + \mathbf{E}_S, \tag{6}$$

where $\mathbf{E}_S = [\boldsymbol{\varepsilon}_S(1), \boldsymbol{\varepsilon}_S(2), \cdots, \boldsymbol{\varepsilon}_S(M)]$.

The problem of the hybrid resolution spectral imaging is to estimate $\mathbf{F} \in \mathbb{R}^{L \times N}$ from its linear observations $\mathbf{G} \in \mathbb{R}^{B \times N}$ and $\mathbf{S} \in \mathbb{R}^{L \times M}$, under the conditions that $B < L$ and $M < N$.

Class-based regression method for mixed low-resolution spectral data [12]

The method consists of the following three steps.

Step 1: RGB image segmentation: The pixels of a high-resolution RGB image are classified into K classes to obtain a segmented RGB image.

Step 2: Extraction of class-based estimation matrices: Based on a regression technique, class-based estimation matrices are extracted from a low-resolution spectral image and the segmented RGB image.

Step 3: High-resolution spectral image reconstruction: The spectral image is estimated pixel by pixel from the segmented RGB image by means of the class-based estimation matrices.

The *Step 2* is explained in detail below. As a result of the classification of *Step 1*, every $\mathbf{g}(i)$ is assigned to one of the K classes. Let $\mathbf{A}_{\#k}$ be an class-oriented estimation matrix from $\mathbf{g}(i)$ to $\mathbf{f}(i)$ if the pixel is assigned to class #k:

$$\hat{\mathbf{f}}_{\#k}(i) = \mathbf{A}_{\#k} \mathbf{g}(i) \mid k, \tag{7}$$

where $\mathbf{g}(i) \mid k$ represents that $\mathbf{g}(i)$ is assigned to class #k.

To derive $\mathbf{A}_{\#k}$, we introduce several new variables:

$$\widetilde{\mathbf{g}}(i) = \begin{pmatrix} \delta_{i1} \mathbf{g}(i) \\ \vdots \\ \delta_{iK} \mathbf{g}(i) \end{pmatrix}, \tag{8}$$

$$\delta_{ik} = \begin{cases} 1 & if \quad \mathbf{g}(i) \in class\#k \\ 0 & else \end{cases}, \tag{9}$$

$$\widetilde{\mathbf{G}} = [\widetilde{\mathbf{g}}(1), \cdots, \widetilde{\mathbf{g}}(N)]. \tag{10}$$

The vector $\widetilde{\mathbf{g}}(i)$ is a KB-dimensional column vector and the matrix $\widetilde{\mathbf{G}}$ is a $(KB) \times N$ matrix.

By using these variables, Eq. (7) can be rewritten as

$$\hat{\mathbf{f}}_{\#k}(i) = \widetilde{\mathbf{A}} \widetilde{\mathbf{g}}(i), \tag{11}$$

where $\widetilde{\mathbf{A}}$ is an $L \times (KB)$ matrix described by

$$\widetilde{\mathbf{A}} = [\mathbf{A}_{\#1} \quad \cdots \quad \mathbf{A}_{\#K}]. \tag{12}$$

To perform the regression estimation based on Eq. (11), the low-resolution version of $\widetilde{\mathbf{G}}$ is calculated as

$$\widetilde{\mathbf{T}} = \widetilde{\mathbf{G}} \mathbf{H}_S, \tag{13}$$

where $\widetilde{\mathbf{T}}$ becomes a $(KB) \times M$ matrix. The j-th column vector of $\widetilde{\mathbf{T}}$, $\widetilde{\mathbf{t}}(j)$, implicitly contains the information about the ratio of the spectra of each class mixed in the j-th spectral data $\mathbf{s}(j)$. In addition, the relation between $\mathbf{s}(j) \Leftrightarrow \widetilde{\mathbf{t}}(j)$ is approximately same as that of $\mathbf{f}(i) \Leftrightarrow \widetilde{\mathbf{g}}(i)$. Therefore, by using $\mathbf{s}(j) \Leftrightarrow \widetilde{\mathbf{t}}(j)$ pairs as training data, the regression estimation matrix $\widetilde{\mathbf{A}}$ is obtained by minimizing
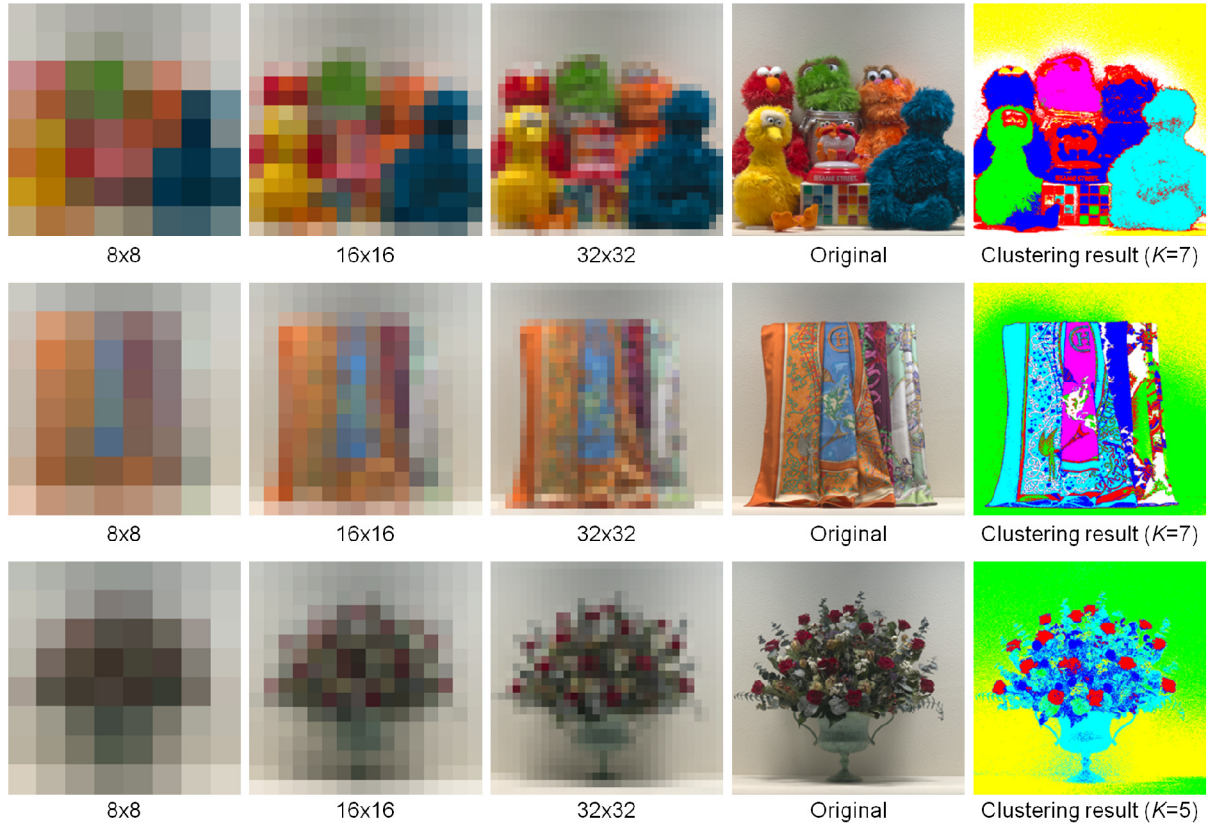
Figure 2. For three test images, Toys, Scarf, and Flower, from top down, low-resolution spectral reflectance images shown in color images with 8x8, 16x16, and 32x32 resolution, Original spectral reflectance images shown in color images, and clustering results, from left to right.

$$\Phi_{unmix} = \sum_{j=1}^{M} \left\| \mathbf{s}(j) - \widetilde{\mathbf{A}}\widetilde{\mathbf{t}}(j) \right\|_2 \;, \tag{14}$$

if $KB << M$. The solution is given by

$$\widetilde{\mathbf{A}} = \mathbf{S}\widetilde{\mathbf{T}}^T \left(\widetilde{\mathbf{T}}\widetilde{\mathbf{T}}^T \right)^{-1} \;. \tag{15}$$

By substituting Eq. (15) into Eq. (11), we estimate the high-resolution spectral image by class-oriented estimation matrices.

Experiments
Data

We prepared three 512×512 spectral reflectance images consisting of 61 wavelength samplings in the range of 380 to 680 nm with an interval of 5 nm. These spectral reflectance images were obtained with the Wiener estimation from a multispectral image captured by a sixteen-band camera [13]. The images are presented in color images in Fig. 2 (second column from right). We call them "Toys", "Scarf", and "Flower".

Two types of observations were assumed from each of the test spectral images. High-resolution RGB images were calculated from the spectral reflectance images using the spectral sensitivity of a typical HDTV video camera and the spectrum of the CIE standard illuminant D65. For simulating noise, Gaussian random white noise was added to the image data, where the peak-signal-to-noise ratio (PSNR) was set at 50 dB.

Each spectrum in the low-resolution spectral data was generated as the average spectrum of a rectangle region whereas the averaging regions neither overlapped nor are separated. The number of pixels of the low-resolution spectral data is 8×8 , 16×16 , and 32×32 . The low-resolution spectral data are shown in color images in left three columns in Fig. 2 to demonstrate the size of the pixel of the low-resolution spectral data. It can be seen that the colors in the small region in the test images of "Scarf" is nearly lost in the low-resolution data while the typical colors in the test images of "Toys" are sufficiently recognized in the low-resolution data. In the case of "Flower", red colors of the roses are lost by averaging with the green colors of the leaves especially for the 8×8 resolution.

Estimation methods

We compared the class-based regression method with two conventional methods for hybrid resolution spectral imaging.

The first is Wiener estimation [3], where the spectral correlation matrix $\mathbf{R}$ is calculated using the low-resolution spectral data:

$$\mathbf{R} = \frac{1}{M} \sum_{j=1}^{M} \left\{ \mathbf{s}(j)\mathbf{s}(j)^T \right\} = \frac{1}{M} \mathbf{S}\mathbf{S}^T \;, \tag{16}$$

The second method is Piecewise Wiener (PW-Wiener) estimation [4]. High-resolution RGB images are divided into blocks, where each block is indexed by q $(1 \le q \le Q)$, and the estimation is performed by the estimation matrix defined for every

©2011 Society for Imaging Science and Technology

block. Each estimation matrix is calculated using the Wiener estimation theory. The spectral correlation matrix for block q, $\mathbf{R}_q$, is calculated using the low-resolution spectral data that are weighted according to the Euclidean distance $d(q,j)$ between the center position of block q and the center position of low-resolution spectral data $\mathbf{s}(j)$:

$$\mathbf{R}_q = \frac{1}{\sum_{j=1}^{M} w(q,j)^2} \sum_{j=1}^{M} \left\{ w(q,j)^2 \mathbf{s}(j)\mathbf{s}(j)^T \right\}, \qquad (17)$$

$$w(q,j) = \rho^{d(q,j)}, \qquad (18)$$

where ρ was set to 0.7. In the implementation, to avoid discontinuities at the block boundary, the estimation of a pixel is performed using the matrix assigned to its neighboring blocks as well as its own block; these are summed by using a two-dimensional Hamming window.

In class-based regression method, segmentation of high-resolution RGB images was performed based on two dimensional (r, g) signals defined by

$$r = \frac{R}{R+G+B}, g = \frac{G}{R+G+B} \ , \qquad (19)$$

because (r, g) signals are independent to power of spectra. The clustering was based on Gaussian mixture model (GMD); the probability density of GMD is estimated to fit sampled data by using an expectation maximization algorithm, and each data are assigned to a class, based on the estimated posterior probability. The number of the clusters K is defined based on Akaike information criterion which is a measure of the relative goodness of fit of a statistical model: $K = 7$ for "Toys" and "Scarf", and $K = 5$ for "Flower". The segmentation results are shown in rightmost column in Fig. 2. Note that other color spaces or textural information can be used for the clustering, but normalization such as Eq. (19) will be required to obtain the similar results.

Results

Below, we use the capital letters for the colors in the segmentation images: R (red), G (green), B (blue), Y (yellow), C (cyan), M (magenta), W (white), while the name of colors are used without abbreviation for the actual colors, as red, green, and orange, etc. In addition, we call three methods Wiener, PW-Wiener, and class-based regression.

Figure three shows the results for three test images. The accuracy of the estimated spectral reflectance images are measured by the average of CIELAB error under F7. The error is calculated for whole image and respective class. Moreover, the number of pixels included in each class is presented with a bar graph (right axis). The horizontal color bar shows the corresponding color of each class in the segmentation images. Figure four shows error images of 200×200 regions for three methods in the case of the 16×16 resolution of the low-resolution spectral data. The regions are selected to include the classes which show the differences in accuracy between the methods in the results of Fig. 3. The range of 0–20 of CIELAB error was allocated to 8-bit grayscale. Below, the results of Figs. 3 and 4 are discussed for every test image.

Toys: Fig. 3 shows that the large errors by Wiener for #5(C) and #6(M) are reduced by both PW-Wiener and class-based regression, regardless of the resolution of the low-resolution

spectral data. In addition, for all classes, PW-Wiener and class-based regression gave similar accuracy. This is because the spectra in the low-resolution spectral data well represent the original spectra, without mixing spectra from different classes. Therefore, it can be said that PW-Wiener and class-based regression are approximately equivalent and better than Wiener in the case of unmixed spectra. The error images in Fig. 4 support this result.

Scarf: Fig. 3 shows that the large errors by Wiener and PW-Wiener for #7(W) are effectively reduced by class-based regression. From the clustering results in Fig. 4, we can see that the class #7(W) consists of the narrow lineal areas in green on the orange background and other small green areas. As a result, the spectral information of these areas should be almost lost in the low-resolution spectral data. Nonetheless, class-based regression realizes high accuracy, which is considered as the effect of spectral unmixing. For class #6(P), relatively large error occurs by class-based regression in the case of the 8×8 resolution of the low-resolution spectral data. We think that this is caused by two factors: first is that the number of pixels in the class is relatively small, and the second is that the number of the data for the regression ($M \times M = 8 \times 8 = 64$ in this case) is not sufficient compared to the number of unknowns ($B \times K = 3 \times 7 = 21$ in this case). Therefore, the number of classes should be selected not only by appropriateness of the clustering but also the resolution of the low-resolution spectral data; if the resolution is low, large number of classes cannot be used.

Flower: Fig. 3 shows that the large errors by Wiener and PW-Wiener for #1(R) are effectively reduced by class-based regression. From the clustering results in Fig. 4, we can see that the class #1(R) corresponds to the red roses on the green background. Considering the size of the roses, spectral information of roses are almost lost in the low-resolution spectral data especially for 8×8 resolution. As a result, large errors occur by Wiener and PW-Wiener. Nonetheless, class-based regression realizes high accuracy, which indicates that class-based regression has the effect of spectral unmixing.

Conclusions

In this paper, class-based regression method for mixed low-resolution spectral data was applied to reconstruct three spectral images. The estimation accuracy was evaluated for every class and compared to two conventional methods for hybrid resolution spectral imaging. As a result, it can be confirmed that class-based regression method works effectively for full-size images without any prominent problems. In addition, evaluation results show that PW-Wiener estimation method and class-based regression method are almost equivalent and better than Wiener estimation method when the low-resolution spectral data are not the mixture of the spectra from different classes; namely, when the spatial configurations of scenes are rough. Otherwise, i.e., fine spectral configurations exist in the scenes, relatively large error can occur in specific classes by Wiener and PW-Wiener estimation methods, while this error is effectively reduced by class-based regression method. Therefore, we can conclude that class-based regression method has the effect of spectral unmixing for mixed low-resolution spectral data even when it is applied to full-size images.
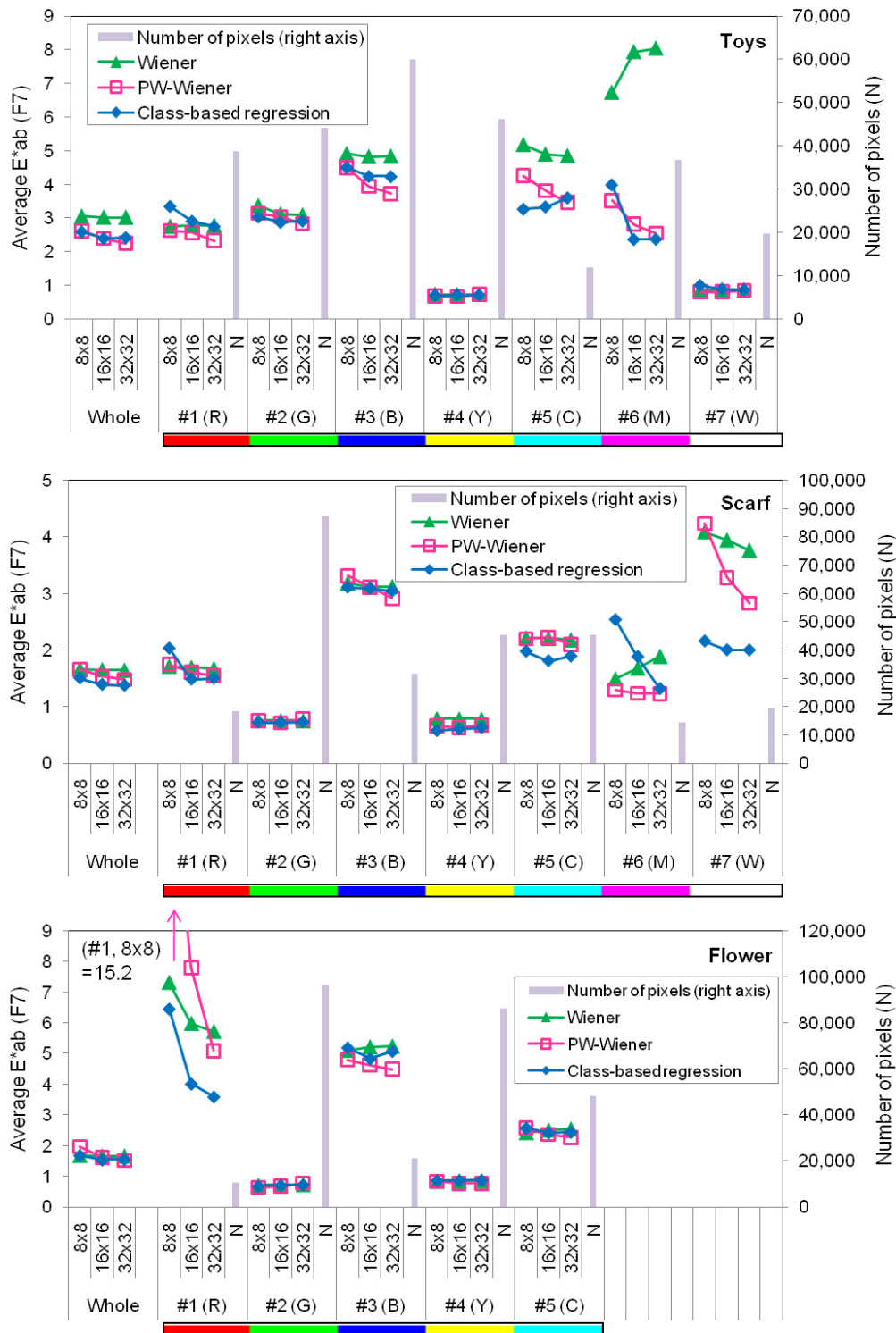
Figure 3. Simulation results for three test images, Toys, Scarf, and Flower, from top to bottom. Plots are average E*ab under F7 illumination for whole images and respective class by three methods. The number of pixels included in each class is presented in bar graph (right axis).
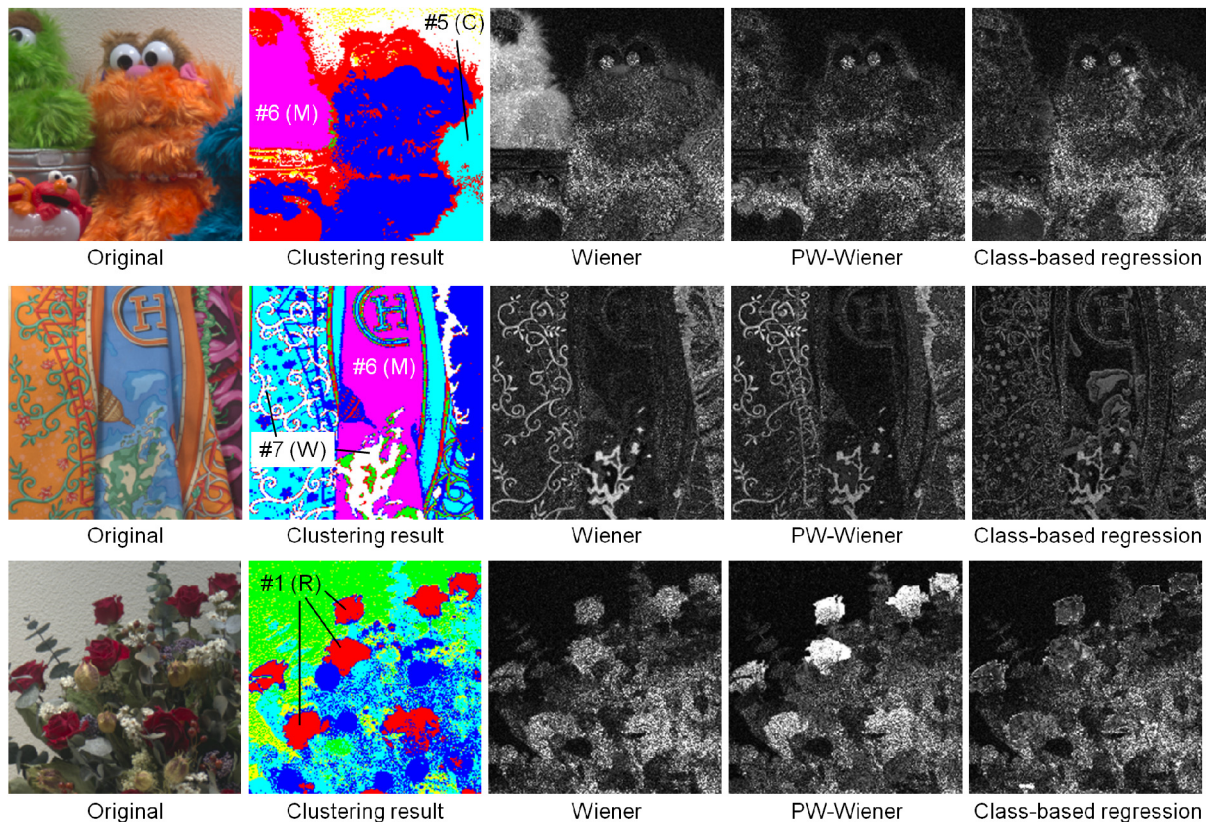
Figure 4. *Error images for 200x200-pixel regions for three test images, Toys, Scarf, and Flower, from top down, in the case of 16x16 resolution of low-resolution spectral data. From left to right, original color images, clustering results, and error images for three methods. The range of 0–20 of CIELAB error was allocated to 8-bit grayscale.*

References

[1] F. H. Imai and R.S. Berns, High-Resolution Multi-Spectral Image Archives: A Hybrid Approach, Proc. CIC, pg. 224 (1998).

[2] Y. Murakami, K. Ietomi, M. Yamaguchi, and N. Ohyama, "MAP Estimation of Spectral Reflectance from Color Image and Multipoint Spectral Measurements," Appl. Opt. 46, 7068 (2007).

[3] Y. Murakami, K. Ietomi, A. Tadano, M. Yamaguchi, and N. Ohyama, Comparison of Spectral Image Reconstruction Methods Using Multipoint Spectral Measurements, Proc. CGIV, pg. 591 (2008).

[4] Y. Murakami, M. Yamaguchi, and N. Ohyama, "Piecewise Wiener Estimation for Reconstruction of Spectral Reflectance Image by Multipoint Spectral Measurements," Appl. Opt. 48, 2188 (2009).

[5] O. Kohonen, Multiresolution-Based Pansharpening in Spectral Color Images, Proc. CGIV, pg. 535 (2010).

[6] J. C. Price, "Combining Panchromatic and Multispectral Imagery from Dual Resolution Satellite Instruments," Remote Sens. Environ. 21, 119 (1987).

[7] D. P. Filiberti, S. E. Marsh, and R. A. Schowengerdt, "Synthesis of Imagery with High Spatial and Spectral Resolution from Multiple Image Sources," Opt. Eng. 33, 2520 (1994).

[8] M. T. Eismann and R. C. Hardie, "Hyperspectral Resolution Enhancement Using High-Resolution Multispectral Imagery with Arbitrary Response Functions," IEEE Trans. Image Processing 43, 455 (2005).

[9] A. Santos-Garcia, M. Velez-Reyez, S. Rosario-Torres, and J. D.Chinea, A Comparison of Unmixing Algorithms for Hyperspectral Imagery, Proc. SPIE 7334, pg. 73341N (2009).

[10] B. Zhukov, D. Oertel, F. Lanzl, and G. Reinhackel, "Unmixingbased Multisensory Multiresolution Image Fusion," IEEE Trans. Geosci. Remote Sens., 37, 1212 (1999).

[11] R. Zurita-Milla, J. G. P. W. Clevers, and M. E. Schaepman, "Unmixing-Based Landsat TM and MERIS FR Data Fusion," IEEE Geosci. Remote Sens. Lett., 5, 453 (2008).

[12] Y. Murakami, M. Yamaguchi, and N. Ohyama, "Class-Based Spectral Reconstruction Based on Unmixing of Low-Resolution Spectral Information," JOSA A, 28, 1470 (2011).

[13] H. Fukuda, T. Uchiyama, H. Haneishi, M. Yamaguchi, and N. Ohyama, Development of 16-band Multispectral Image Archiving System, Proc. SPIE 5667, 136 (2002).

Author Biography

Yuri Murakami is a research fellow of the Japan Society for the Promotion of Science, at Imaging Science and Engineering Laboratory, Tokyo Institute of Technology (Tokyo Tech), Japan. She received her M. S. and Ph. D. degrees from the Tokyo Tech in 1998 and 2005, and in 2000-2005 she was an assistant professor at Tokyo Tech. Her research interests include multispectral imaging, color image reproduction.